Eur. Phys. J. B **7**, 155–168 (1999)

THE EUROPEAN PHYSICAL JOURNAL B

EDP Sciences

On the validity of Hertz contact law for granular material acoustics

C. Coste[a] and B. Gilles

Laboratoire de Physique, École Normale Supérieure de Lyon, 46 allée d'Italie, 69364 Lyon Cedex 07, France

Revised: 28 May 1998 / Accepted: 27 July 1998

Abstract. We discuss the acoustical behavior of a 1D model of granular medium, which is a chain of identical spherical beads. In this geometry, we are able to test quantitatively alternative models to the Hertz theory of contact between elastic solids. We compare the predictions of the different models to experimental results that concern linear sound wave propagation in the chain submitted to a static force, and nonlinear solitary wave propagation in an unconstrained chain. We use elastic, elastic-plastic and brittle materials, the beads roughness extends on one order of magnitude, and we also use oxidized metallic beads. We demonstrate experimentally that at low static forces, for all types of beads, the linear acoustic waves propagate in the system as predicted by Hertz's theory. At larger forces, after onset of permanent plastic deformation at the contacts, the brass beads exhibit non Hertzian behavior, and hysteresis. Except in the case of brass beads, the nonlinear waves follow the predictions of Hertz theory.

PACS. 83.70.Fn Granular solids – 83.10.Pp Particle dynamics – 43.25.Cb Macrosonic propagation, finite amplitude sound; shock waves

1 Introduction

Granular materials are very common and widely spread, both in geophysical or industrial contexts. In this respect, acoustical methods are very useful investigation tools, and sometimes the only one available. They allow analysis of otherwise inaccessible geophysical materials, nondestructive control in industrial situations, and measurements of dynamical properties in the laboratory. The description of sound waves propagation in granular materials is thus a problem of fundamental interest.

Those materials are assemblies of grains, and the understanding of their dynamical behavior is a complicated many body problem. Indeed, it depends on a huge number of parameters. A first set characterizes the statistical distributions of shape, size and constitutive materials of the grain assembly. The second set is linked to the fact that wave propagation obviously takes place along the contacts between the grains. Consequently, one must include the parameters that describe the dynamical behavior of individual contacts, and the geometry of the contact lattice.

Experimental works were initiated by Iida [1,2] on sand, and the contacts between grains were ensured by gravity. Other investigations were concerned with the propagation of seismic waves in materials submitted to very high pressures [3–5], a rather complicated situation in which fracturation of grains happened. Recently, Liu and Nagel studied sound propagation in sand, focusing on geometrical effects due to the disorder of the piling [6,7].

[a] e-mail: coste@physique.ens-lyon.fr

In all those experiments the individual properties of the grains themselves were rather complicated. The simplest granular assemblies are pilings of identical spherical beads. In that case, every distribution of grain properties is a Dirac function, and the acoustic behavior of the medium depends only on the contacts. The interaction law between two adjacent elastic spheres is an exact solution of linear elasticity, known as the Hertz's law [8]. It predicts that the relation between the force F_0 exerted on the spheres and the distance of approach of their centers, δ_0, is nonlinear, $F_0 \propto \delta_0^{3/2}$. The nonlinearity comes from purely geometric effects. As a consequence of the Hertz's interaction law, the sound velocity c_s in the bead lattice should depend on the static force as a power law, $c_s \propto F_0^{1/6}$ [9]. In one dimension, the nonlinear behavior of a bead chain has been described by Nesterenko [10,11]. Assuming Hertz contact between adjacent beads, he proved the possibility of solitary waves propagation.

In 1D systems, the existence of those nonlinear excitations have been experimentally demonstrated [12,13], in quantitative agreement with the theoretical predictions. The case of linear acoustic waves is more controversial. The 1/6 exponent have been observed in 1D systems (a chain of spherical beads) [14], but spherical bead pilings of higher dimensionality display more complicated features. The case of 3D pilings have been thoroughly reviewed by Goddard [15], and it appears that the data rather correspond to an exponent 1/4.

Two strategies may be invoked to explain this discrepancy. A *microscopic* approach will focus on individual contacts between the grains, and search for non Hertzian behavior of the contacts, due to deviation of actual beads from perfectly smooth and homogeneous elastic spheres. A more *macroscopic* way to tackle the problem compares the lattice of actual, active contacts, to the bead center lattice.

Actual beads, used in real experiments, differ from the ideal ones considered by Hertz in several respects. They are certainly not perfectly smooth, neither spherical, they may be inhomogeneous and exhibit plastic deformations. The unavoidable roughness of real beads led Goddard [15] to study the interaction between *conical* microcontacts, that should modelize the asperities of the beads. De Gennes [16,17] takes into account two other different possible causes of non Hertzian behavior. In a first model [16], he considers the effect of a thin oxide layer at the surface of the beads. Metallic oxides are not particularly soft, but the layers that developpe on metals are porous, and may greatly modify the mechanical properties of contacts. In another model [17], he looked for plastic deformation of microcontacts, that is contacts between the small asperities of the rough adjacent surfaces. Because of the smallness of the asperities, plasticity may intervene even at very small applied forces. All those models predict a power law with exponent 1/4 for the sound velocity as a function of the static force applied on the piling.

The other approach, that depends on collective behavior of the grains, has been proposed by S. Roux *et al.* [18–20]. The idea is the following. Since contacts between spheres (or disks in 2D numerical experiments) are point contacts, even a small scatter in diameter distribution implies that some contacts are broken. The contacts that still transmit normal stresses, or waves, are called *active* contacts. The *collective* behavior of the piling may thus be modified: even if the lattice of the bead centers is perfect, the lattice of the active contacts is disordered, and the effective compressibility of the piling do not follow the Hertz law, although the individual active contacts do. Experimental observations of 2D regular pilings of plexiglass cylinders in photoelasticity support this idea [21, 22]. This analysis have been validated by numerical simulation on small systems [18–20], and recently it has been confirmed on much larger systems [23,24]. In the reference cited [15], Goddard developed a macroscopic model, based on the variation in the number density of Hertzian contacts, due to buckling of particle chains. Those model also give 1/4 as the power law exponent. Accordingly, it is impossible to distinguish the relevant physical mechanism with experiments in 2D or 3D pilings.

In this paper, we report on quantitative experiments on both linear and nonlinear waves in a 1D system, which is a chain of identical spherical beads of several different materials. The contact lattice, in 1D, is as regular as the center lattice, and we are free from the collective effects linked to geometry of contact lattice in higher dimensions. Consequently, properly choosing the bead materials, we are able to test the different microscopic models [15–17] that assume a modified Hertz law for the contact between grains. We demonstrate experimentally that those models are not relevant to the description of our experiments, which indicates that departure from Hertz behavior may come from collective effects rather than non Hertzian behavior of individual contacts, at least for small static force.

At higher forces, we observe non Hertzian behavior in chains of brass beads. In logarithmic scales, when the force is increased, the velocity is still a linear function of the force, but the slope is 0.22 rather than 1/6. When the static force is decreased, there is an hysteretic effect since the velocity follows a third line, of slope 1/7. Brass is a rather plastic alloy, and the force at the transition corresponds to the onset of permanent plastic deformation of the contact area. This concerns the deformed part of the beads in Hertz theory, not microcontacts between asperities.

The paper is organized as follows. Section 2 is devoted to a sketchy presentation of the relevant theoretical analysis, since details may be found elsewhere [10,11,13]. The experimental apparatus is described in Section 3, and the methods used for data analysis in Section 4. The experimental results are exposed in Section 5, and discussed in Section 6. Finally we conclude in Section 7.

2 Theoretical analysis

In this section, we give only the essential informations concerning the theoretical modeling of our experimental system. The details of the calculations may be found in the original papers of Nesterenko [10,11], who first demonstrate the existence of solitary waves in such systems, or in [13].

The contact interaction of adjacent beads is described by the relation between the static force F_0 applied on the beads and the distance of approach δ_0 of their centers. We consider either the Hertz Law, hereafter HL, for which

$$F_0 = \frac{2\theta}{3}\sqrt{\frac{a}{2}}\,\delta_0^{3/2}, \quad \theta \equiv \frac{E}{1-\nu^2}, \tag{1}$$

or the Modified Hertz Law, hereafter MHL, for which

$$F_0 \propto \delta_0^2, \tag{2}$$

where E is the Young's modulus, ν the Poisson's coefficient and a the radius of the beads, which are supposed to be identical. The theoretical analysis leading to the MHL are scaling theories, and give no analytic expression for the proportionality constant in (2). In the following analysis, we will thus be concerned mainly by the search of power laws, and the measurement of their exponents.

Those interaction laws are valid when the contacts are submitted to a *static* constraint, but we will use them in dynamic problems when the force between neighbouring beads evolves with time. This *quasistatic* approximation is justified by the experimental times scales, that are always much smaller than the travel time of a *bulk* acoustic wave along a bead diameter. The order of magnitude of this

travel time is $2\,\mu$s, whereas the period of acoustic waves is $100\,\mu$s (see Sect. 3.2) and the duration of a solitary wave $30\ \mu$s (see Fig. 11).

The elastic or plastic deformation of the beads is concentrated in a very narrow region around the contact point. The chain is thus well described as a chain of point masses $m = 4\pi\rho a^3/3$, where ρ is the bead density, linked by nonlinear springs with a force-displacement relation given either by (1), for the HL, or (2), for the MHL. Denoting by u_n the displacement of the nth bead from its equilibrium position, the dynamics of the chain is described by a system of coupled differential equations

$$\ddot{u}_n = A_\alpha \left\{ \Big[\delta_0 - (u_n - u_{n-1})\Big]^\alpha - \Big[\delta_0 - (u_{n+1} - u_n)\Big]^\alpha \right\},$$
$$A_H = \frac{\theta}{2\pi\sqrt{2}a^{5/2}\rho}, \quad \alpha = \frac{3}{2} \qquad \text{(HL)} \tag{3}$$
$$A_{MH} \text{ unspecified}, \quad \alpha = 2 \qquad \text{(MHL)}.$$

In the *linear* case, $|u_{n+1} - u_n| \ll \delta_0$, we recover the usual model of a chain of identical point masses linked by identical linear springs, and the speed of sound in the chain is

$$\begin{cases} c_s = C_H F_0^{1/6} \quad C_H \equiv \frac{3}{2\sqrt{\pi\rho}} \left(\frac{4\theta}{3a}\right)^{1/3} & \text{(HL)} \\ c_s = C_{MH} F_0^{1/4}, \quad C_{MH} \text{ unspecified} & \text{(MHL)} \end{cases} \tag{4}$$

so that, in both cases, there is no linear sound propagation when no static force is applied on the chain, that is when $F_0 = 0$.

Another useful approximation of equation (3) is the strongly nonlinear case $|u_{n+1} - u_n| \gg \delta_0$, in the continuous limit when the typical size of the excitations, say L, is much greater than a. We write $u_n(t) = u(x,t)$, the *total* displacement of the bead centers (including the one due to the static force), where x is the abscissa along the chain, and obtain from (3), up to order $(a/L)^2$,

$$u_{tt} = -D_\alpha^2 \Big\{ (-u_x)^\alpha + \frac{\alpha a^2}{6} \Big[(\alpha-1)(-u_x)^{\alpha-2} u_{xx}^2 - 2(-u_x)^{\alpha-1} u_{xxx} \Big] \Big\}_x, \tag{5}$$
$$D_H^2 = \frac{2\theta}{\pi\rho}, \quad \alpha = \frac{3}{2} \qquad \text{(HL)}$$
$$D_{MH} \text{ unspecified}, \quad \alpha = 2 \qquad \text{(MHL)}.$$

We look for progressive waves $u(\xi \equiv x - Vt)$, where the wave velocity V is to be determined, and set $\psi = -u_\xi$. The equation (5) is easily integrated to give

$$\frac{V^2}{D_\alpha^2}(\psi - \psi_\infty) = \psi^\alpha - \psi_\infty^\alpha + \frac{\alpha a^2}{6}\Big[(\alpha-1)\psi^{\alpha-2}\psi_\xi^2 + 2\psi^{\alpha-1}\psi_{\xi\xi}\Big], \tag{6}$$

where ψ_∞ is the displacement gradient at infinity. We search for a localized excitation, so that $\psi_\xi \to 0$ when $\xi \to \pm\infty$. Making the change of variables

$$y = \left(\frac{V}{D_\alpha}\right)^{\frac{\alpha+1}{1-\alpha}} \psi^{\frac{\alpha+1}{2}}, \quad \eta = \frac{\xi}{a}\sqrt{\frac{3(\alpha+1)}{2\alpha}}, \tag{7}$$

we get [11]

$$y_{\eta\eta} \equiv -\frac{dW(y)}{dy} = -\frac{d}{dy}\left[\frac{1}{2}y^2 - \frac{\alpha+1}{4}y^{\frac{4}{\alpha+1}} - \frac{\alpha+1}{2}y^{\frac{2}{\alpha+1}}\left(y_\infty^{\frac{2\alpha}{\alpha+1}} - y_\infty^{\frac{2}{\alpha+1}}\right)\right]. \tag{8}$$

This equation, in an obvious mechanical analogy, describes the motion of a particle of unit mass at "position" y, in the "potential" $W(y)$, during the "time" η.

The function $W(y)$ always has a maximum at $y = y_\infty$, and a minimum at

$$y_+^{HL} = \left\{ \frac{1}{2}\left[1 - y_\infty^{2/5} + \sqrt{\left(1 - y_\infty^{2/5}\right)\left(1 + 3y_\infty^{2/5}\right)} \right] \right\}^{5/2}, \tag{9}$$

defined for $0 \le y_\infty \le 1$, with

$$y_+^{HL} \ge y_\infty \quad \text{if} \quad 0 \le y_\infty \le \left(\frac{2}{3}\right)^{5/2}, \tag{10}$$

in the HL case, and at

$$y_+^{MHL} = \left(1 - y_\infty^{2/3}\right)^{3/2}, \tag{11}$$

defined for $0 \le y_\infty \le 1$, with

$$y_+^{MHL} \ge y_\infty \quad \text{if} \quad 0 \le y_\infty \le \left(\frac{1}{2}\right)^{3/2}, \tag{12}$$

in the MHL case. In the mechanical analogy, if the particle is initially at y_∞, it goes away from its unstable equilibrium position up to position y_m, defined by

$$W(y_m) - W(y_\infty) = 0, \tag{13}$$

in an infinite time because y_∞ is the location of a maximum of the potential, and then returns to position y_∞ in an infinite time again. Coming back to our wave problem, this describes the propagation of a solitary wave of amplitude y_∞ at $\eta \to \pm\infty$, and of maximum amplitude y_m at $\eta = 0$ (say). Those solitary waves have been predicted by Nesterenko [10,11], and observed experimentally in the Hertz case for which $\alpha = 3/2$ [12,13].

With no static force applied on the chain, there is no displacement gradient at infinity, so that $y_\infty = 0$. This simplification allows an explicit integration of (8), and leads to

$$\psi(x,t) = \begin{cases} \left(\frac{5}{4}\frac{V^2}{D_H^2}\right)^2 \cos^4 \frac{x - Vt}{a\sqrt{10}} & \text{(HL)} \\ \frac{3}{2}\frac{V^2}{D_{MH}^2} \cos^2 \frac{x - Vt}{2a} & \text{(MHL)}. \end{cases} \tag{14}$$

Table 1. Tolerance specifications of the beads

Bead material	Diameter (μm)	Sphericity (μm)
Stainless Steel	± 4	± 2
Brass	± 20	± 10
Glass	± 20	± 20
Nylon	± 50	± 25

In the limiting case of no static force applied on the chain, we do not recover solitary waves, but rather nonlinear periodical waves [11]. This limit is mathematically singular, because solitary waves do exist for any nonzero static force, however small. Most importantly, as shown in [13], the limiting shape of the solitary wave when the static force tends to zero is one arch of the periodical wave (14). This is confirmed by direct numerical simulations of (3), in the Hertz case, where solitary wave propagation have been observed by Nesterenko [10] in a chain without static force. Solitary waves in a chain of steel beads under no static force have also been observed experimentally in [13], and a very good agreement is found with the theoretical predictions, both for the shape and the velocity of the wave. This configuration is also particularly important to discriminate between the HL and the MHL, as shown by (14) for the wave profile, and by (18, 20) for the wave velocity. This point is emphasized in Section 4.

3 Experimental setup

We study experimentally the acoustical behavior of a 1D chain of identical spherical beads. In order to discard any geometrical effect, great care is taken in the realization of the device that ensures alignment of the beads in the chain. This system allows an unambiguous test of the different microscopic theories leading to the MHL. To this end, we use beads of different kinds, with mechanical behaviors that may be of concern to the various mechanisms that are at the basis of the three different versions of MHL. Their characteristics are detailed in Section 3.1 below. We use similar, but not identical setups for the study of linear and nonlinear waves. They are described in Sections 3.2 and 3.3.

3.1 Bead characteristics

Our aim in this paper is to test several different alternative theories to the Hertz theory of solid bodies in contact. They all predict that the sound velocity in a chain of beads in contact under a static force F_0 scales as $F_0^{1/4}$, rather than $F_0^{1/6}$ as predicted by Hertz, but the relevant physical mechanisms are rather different.

In his first model [16], De Gennes considers that for metallic beads, a thin oxidized layer is responsible for a discrepancy with the HL. In order to test this prediction, we use brass beads (60% Cu, 40% Zn), that are furnished with a clean and polished surface (see specifications in Tab. 1). We oxidate some beads by putting them during six hours in a solution of Nitric acid 0.1 M; they will be called hereafter *oxidized brass* beads. Oxidation of the other brass beads is completely negligible in comparison, during the completion time of the experiments. We also use stainless steel, glass and nylon beads for which we are sure that no oxidation occurs. The prediction of the model in reference [16] is that the chain of oxidized brass beads should behave differently than the others.

Table 2. Material properties of the beads. Data for steel and brass are taken from reference [31], data for Nylon from references [29,32], data for glass from [32].

Signification	Young modulus	Poisson's coefficient	Density
Symbol	E	σ	ρ
Unit	N/m^2	–	kg/m^3
Stainless steel	2.26×10^{11}	0.3	7650
Brass	1.04×10^{11}	0.37	8600
Glass	6.2×10^{10}	0.24	2500
Nylon	3.55×10^{9}	0.4	1140

The second De Gennes model [17] attributes to local plastic deformations at microcontacts the deviation from the HL. We use beads in several plastic materials, stainless steel, brass and nylon, in order of decreasing yield stress (see Tabs. 2 and 4 for numerical values of relevant physical constants), and beads of glass, a brittle material. A result of our experiments is that plasticity has indeed an effect on the dynamics of the chain, both for linear and nonlinear waves, although not really in the sense of De Gennes predictions. This point is discussed at length in Section 6.

In his model, Goddard [15] uses classical linear elasticity theory, but for conical contacts. Physically, deviations from perfectly smooth and spherical surface may be responsible for a discrepancy between HL and actual behavior of solid bodies in contact. Obviously, all beads, whatever their material, do have non ideal spherical shapes, and are candidates for this model. However, the deviation from perfect sphericity depends strongly on the beads materials. As shown in Table 1, the tolerance for asphericity ranges from $\pm 2\,\mu$m for steel beads up to $\pm 25\,\mu$m for nylon beads. In some experiments, fracturation of the glass beads occurs, which increases the probability of conical contacts apparition.

Let us summarize the respective properties of the various types of beads used in our experiment:

- Stainless steel beads are the most spherical and less plastic ones, and its no surprise if their behavior is in excellent agreement with HL. This confirms, and extends, previous results of reference [13].
- Brass beads are less spherical, much more plastic,

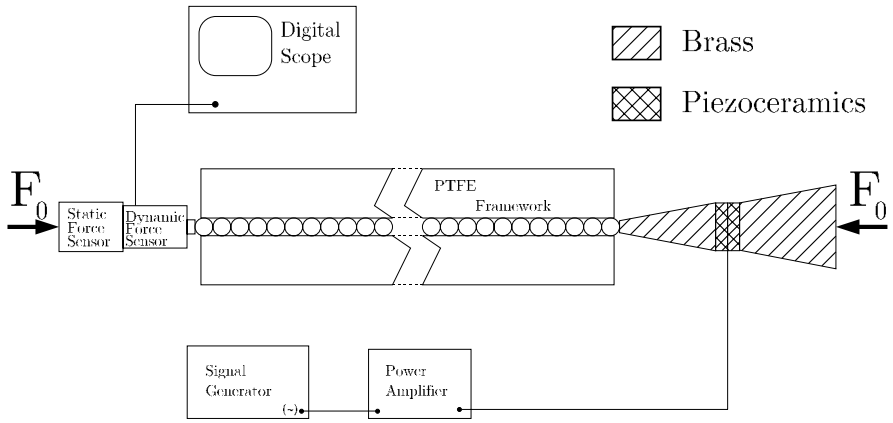

Fig. 1. Sketch of the experimental setup. The sound emitter is on the right hand side; it consists in two coaxial and cross polarized piezoceramics, sandwiched between two conical brass pieces. At the end of the chain, on the left hand side of the sketch, a dynamic force sensor measures the acoustic signal, and a static force sensor measures the force applied on the chain. Two mechanical devices, not represented, ensure longitudinal displacement of both the emitter and the sensors.

and may easily be oxidized, so that they are relevant for all of the three mechanisms.

• Glass beads are less smooth than the others, but are constituted from brittle material, so that only Goddard's mechanism may intervene to correct HL.

• Nylon beads are the most plastic, and less spherical ones.

3.2 Linear waves

Our experimental setup is quite similar to the one described in reference [13] and is sketched in Figure 1. The chain consists in 51 identical beads, 8 mm in diameter. The material characteristics of the beads are given in Table 2, while their tolerances are given in Table 1. The chain is surrounded by a framework of polytetrafluoroethylene (PTFE). It consists of two parts, each one 30 mm high, 40 mm wide and 400 mm long, with a straight channel of squared cross section, 8.02 mm wide, milled in the lower part, that contains the beads. The sound velocity in bulk PTFE is about 400 m/s, which is less than the sound velocity in the chain. Thus confusion between the signal that propagates in the chain and in the framework is avoided.

The static force applied to the chain is controlled by a static force sensor (FGP Instrumentation$^{\text{TM}}$, of sensitivity 3 mV/N). The longitudinal acoustic signal is detected with a dynamic force sensor (Dytran$^{\text{TM}}$, sensitivity 10 mV/LbF), held at the end of the chain. The alignment of the sensors ensures that they have the same axis as the chain. Sound emission is ensured by a set of two coaxial annular plates of piezoelectric material, longitudinally polarized, with cross polarizations [25]. To increase the signal amplitude, the ceramics are held between two conical pieces of brass [26]. The length of the brass pieces is adjusted in order to set the resonant frequency of the emitter to 10 kHz. This frequency is low enough to stay on the linear part, $\omega = c_s k$, of the dispersion curve for the chain [14]. We thus measure with this apparatus the acoustic velocity c_s, for different applied static forces. The conical shape of the brass concentrators ensures a signal of greatest amplitude on the side with the smallest cross section; this side is kept in contact with the chain, whereas reflection on the other side is reduced. This shape is not the most efficient one, but is by far the easiest to built.

We produce acoustic wave trains, made of 3 (sometimes 5, with no significant difference) oscillations of frequency 10 kHz. The period of wave train emission is 0.1 s, much greater than the time taken by the wave to travel along the chain (1 ms in the worst cases). Each wave train is thus completely damped when the next one is emitted. The time of flight is measured with a digital scope, taking into account emission and reception delays with the help of a first measurement, in which the dynamic force sensor is directly held onto the emitter.

3.3 Nonlinear waves

The setup used to produce and analyze nonlinear solitary waves is described at length in reference [13], so we will be very brief here. The experimental realization of the beads chain is extremely similar to the preceding one. The only modification is that the dynamometer at the end of the chain is replaced by a static force sensor, ensuring a somewhat greater precision.

The high amplitude compressional waves are produced with an impact generator. This device consists in a tungsten carbide bead, which moves freely between the first bead of the chain and a piston that oscillates periodically. The impact with the chain is very brief (typically 50 μs), allowing a large momentum transfer.

The impact creates a longitudinal solitary wave that propagates along the chain. A dynamical force sensor is mounted on the static one, at the end of the chain. It measures the temporal evolution of the wave's amplitude; with the help of a digitizing oscilloscope, we can thus record the complete wave profile on a computer.

Three other dynamical force sensors are held along the chain, in contact with beads 6, 26 and 46 respectively, and measure the force exerted by the bead normally to the chain axis. This transverse force is related in a complex, nonlinear, way to the force exerted along the chain axis [27], so that those sensors give no information about the wave profile. However, they allow velocity measurements, because the time of flight between two sensors is known.

We explain in Section 4 why we mainly look for power laws, and thus make measurements with no static force applied on the chain. In that case, we proceed in the following way: we first apply a force to the chain in order to keep the beads into contact, and only then do we relax it to zero. The impact of the moving tungsten carbide bead creates a solitary wave, that is felt by the first dynamical sensor, which triggers the digitizing oscilloscope. This apparatus allows for pre-triggering, so that we register the arrival of the wave on the first sensor. We thus get all informations about the shape and velocity of the wave. After its arrival at the end of the chain, the beads are separated from each other, and we must again keep them into contact.

4 Data analysis

In this section, we emphasize which experimental tests are most suitable to discriminate between the HL and the MHL, taking into account that the proposed modifications of the Hertz law actually give a power law exponent for the velocity as a function of the force, but not the prefactor [15–17].

In the case of small dynamical excitations, we measure the velocity c_s of long wavelength (compared to the beads radius) acoustic waves, for different values of the static force F_0. The sound emitter described in Section 3.2 is specially designed to send an acoustic signal of low frequency, typically 10 kHz; the cut-off frequency of the chain depends as a power law on the static force too, with the same exponent as the velocity [14], but is at least 30 kHz, ensuring that we actually are in the long waves regime. As shown by (4), $c_s \propto F_0^{1/6}$ for the HL and $c_s \propto F_0^{1/4}$ for the MHL. This allows a clear experimental test, the results of which are displayed below in Section 5.1.

In the case of high amplitude excitations, we focus on the behavior of the chain without any static force. This case is of particular importance for two reasons. First, acoustic wave propagation is impossible in this configuration, and the nonlinear solitary waves are the only excitations that propagate along the chain. This is typical of nonlinear partial differential equations like (5), whatever the value of α, and in contrast with usual models with solitary waves solutions, such as Korteweg-de Vries or Cubic Schrödinger equations [28], that support acoustic wave propagation in the small amplitude limit. This distinctive feature of nonlinear wave propagation in a chain of beads is typical of the contact law, and constitutes a severe test. The second reason is that we can exhibit power laws for the velocity and shape of the wave, as we will see below.

As shown in Section 3, we have access in our experiments to the velocity of the wave, by performing time of flight measurements, and to the time evolution of the force felt by the dynamic force sensor held at the end of the chain. The permanent constraint applied on the chain is measured with a static force sensor. The quantity ψ, which appears in (6) is the gradient of the *total* displacement of the bead center. It is the sum of the constant value at equilibrium, $\psi_\infty = \delta_0/(2a)$, which depends on the static force only and is given by the static force sensor, and a time varying part $\widetilde{\psi}(t)$ which is measured by the dynamic force sensor.

Let us first consider the HL case. We have to take into account that the contact between the sensor and the last bead of the chain is between a plane and a sphere, so that [8]

$$\delta_{plane-sphere} = \delta_{sphere-sphere}/2^{1/3}. \tag{15}$$

Moreover, the contact surface is at a distance a from the center of the bead. Let x_w be the position of the sensor, and δ_w the distance of approach between the sensor and the last bead; we have

$$\delta_w \equiv u(x_w - a) - u(x_w) = -a\left(\frac{\partial u}{\partial x}\right)_{x_w} = a\psi. \tag{16}$$

From those equations, we deduce the relationship between the signal given by the sensor, $F(t)$, of maximum value F_m, and $\widetilde{\psi}(t)$, which reads without static force

$$\widetilde{\psi}(t) = \left(\frac{3}{4a^2\theta}\right)^{2/3} \left[2F(t)\right]^{2/3}. \tag{17}$$

This relation, together with the analytic solution (14) and the definition of D_H in (5), gives an explicit relation between the velocity V_H of the wave and its maximum amplitude F_m,

$$V_H = B_H F_m^{1/6}, \quad B_H \equiv \left(\frac{3}{5\pi\rho}\right)^{1/2}\left(\frac{16\theta}{3a}\right)^{1/3}, \qquad \text{(HL)}. \tag{18}$$

In the MHL case, we can easily show that the solitary wave velocity depends on its maximum amplitude as a power law, and calculate the exponent. Let us drop in (5), written for the $\alpha = 2$, the most derivated terms; we obtain

$$u_{tt} \sim D_{MH}^2(-u_x)u_{xx} \tag{19}$$

which is a nonlinear wave equation with an amplitude-dependent wave velocity $V_{MH} \sim D_{MH}(-u_x)^{1/2}$. Using the modified Hertz law (2), we may write $(-u_x) \propto F_m^{1/2}$, so that we get

$$V_{MH} \propto F_m^{1/4} \qquad \text{(MHL)}. \tag{20}$$

In a sense, this result is what dimensional analysis predicts for the MHL, because the solitary wave velocity depends on its amplitude in the same way as the acoustic wave

Table 3. Summary of sound velocity measurements, displayed in Figures 2–6. The indicated values for brass beads concern *low static force* only. See Sections 5.1 and 6 for details. The theoretical value of the power law exponent α_l is 1/6 for the HL and 1/4 for the MHL. See Section 2 for other definitions and Section 5.1 for comments on those results.

	C_H^{th}	C_H^{exp}	ϵ	W	α_l^{-1}
Units	m/sN$^{1/6}$	m/sN$^{1/6}$	N	N	–
Stainless steel	422	447 ± 10	2.5	1.0	6.0 ± 0.1
Glass	474	515 ± 14	0.6	0.3	6.0 ± 0.1
Brass	316	353 ± 10	0.1	1.1	6.0 ± 0.1
Oxydated brass	316	342 ± 10	0.1	1.1	6.0 ± 0.1
Nylon	281	278 ± 15	0.0	0.15	6.0 ± 0.1

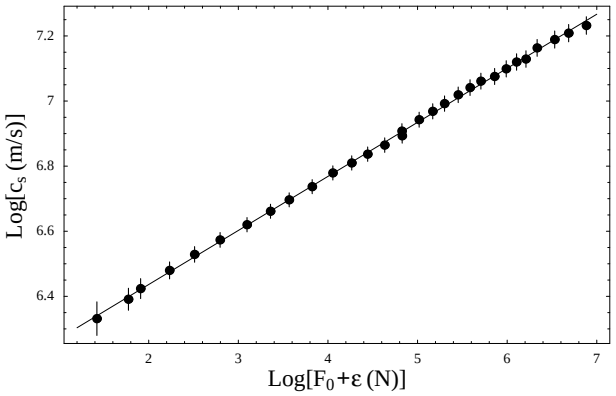

Fig. 2. Logarithmic plot of the sound velocity c_s (in m/s) *versus* the static force applied to the chain $F = F_0 + \varepsilon$ (in N) for a chain of stainless-steel beads. The linearity is good, and the slope of the solid line, fitting the thirty points, corresponds to the equation (23). The values of the exponent α_l, of the residual force ε and of the proportionality coefficient C_H are to be found in Table 3. The static force range is $F_0 \in [5, 974]$ N, and the corresponding sound velocity range $c_s \in [562, 1383]$ m/s.

velocity on the static force. The comparison between the power law relations (18, 20) and the experimental results is done in Section 5.2.

The theoretical expression for the shape of the solitary wave, when no static force is applied on the chain, is one arch of the following nonlinear periodical wave solution, derived from (14),

$$F(t) = F_m \cos^6\left(\frac{V_H(F_m)t}{\sqrt{10}a}\right) \quad \text{(HL)}, \qquad (21)$$

$$F(t) = F_m \cos^4\left(\frac{V_{MH}t}{2a}\right) \quad \text{(MHL)}. \qquad (22)$$

In the HL case, the wave velocity $V_H(F_m)$ is a known function of the maximum amplitude F_m, from equation (18), so that the value of the maximum amplitude gives the complete shape of the wave, without any adjustable parameter. The MHL gives no explicit expression for the velocity V_{MH}; in order to test (22), we take for the velocity the experimental one. The result of the comparison is displayed in Section 5.3.

5 Experimental results

5.1 Velocity of linear acoustic waves

We describe in this section the results of linear velocity measurements, in 1D chains of identical beads made of different materials (stainless steel, glass, brass or oxidized brass, nylon). The experimental setup is described in Section 3.2. We monitor the static force applied on the chain, and we measure the sound velocity for several forces. The evolution of the velocity with the static force is then compared to the prediction of HL and MHL (4).

We display log-log plots of the sound velocity c_s as a function of the static force F_0. It appears that the best fit of the data is

$$c_s = C_H^{exp}(F_0 + \varepsilon)^{\alpha_l}. \qquad (23)$$

The experimental values of the three parameters of the fit, together with the theoretical value C_H^{th} are given in Table 3.

Except for steel beads, the residual force ε is less than the precision of static force measurements, which is typically 1 N. We interpret this small force as an effect of contact between beads and the PTFE framework (solid friction, small local deformation of the framework ...). The order of magnitude is comparable to the weight W of the chain, as shown in Table 3, which supports this interpretation. Given the uncertainty on the static force measurements, the only case of importance is that of stainless-steel beads, for which $\varepsilon = 2.5$ N. It represents a force per bead of 5×10^{-2} N, to be compared to a bead weight of 2.5×10^{-2} N. If we consider that those beads are the ones with higher tolerances, it is no surprise that they all interact with the framework, with a normal force that can be somewhat greater than their weight. In contrast, for beads of other materials, tolerances are poorer, and since we discard too big beads, the mean static interaction with the framework may be smaller.

The sound velocity data are displayed in Figures 2–6. The experimental slopes, together with the coefficient of proportionality in (23), are summarized in Table 3. In all cases except brass at high static force, the numerical value of the exponent α_l is very near its HL value 1/6. The experimental values of the proportionality constants C_H^{exp} are in rather good agreement with HL predictions C_H^{th}, calculated with the data of Table 2, although they seem to be somewhat higher. The physical constants are tabulated for bulk materials, whereas the beads are obtained after complicated and uncontrolled mechanical operations, so that their mechanical properties may be somewhat different from those for bulk materials in large samples. Static measurements of mechanical properties can be done only

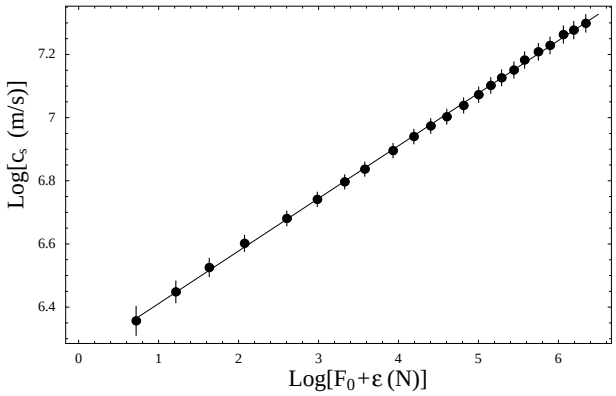

Fig. 3. Same as Figure 2, but for a chain of glass beads. The static force range is $F_0 \in [3, 600]$ N, and the corresponding sound velocity range $c_s \in [563, 1480]$ m/s. The linear fit is in agreement with HL predictions

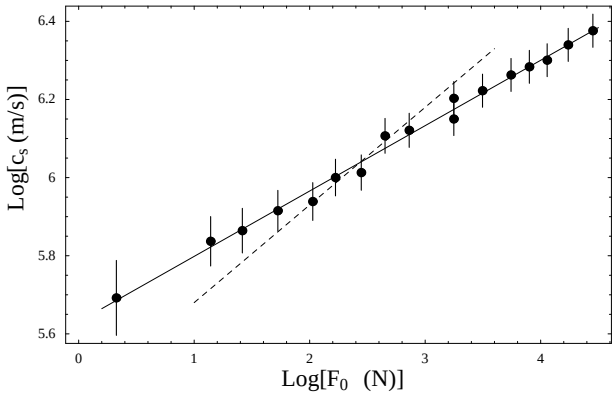

Fig. 4. Same as Figure 2, but for a chain of nylon beads. The static force range is $F_0 \in [2, 90]$ N, and the corresponding sound velocity range $c_s \in [297, 595]$ m/s. The available static force range is smaller than for the other materials; we have thus indicated a dashed line of slope 1/4 which indicates that this exponent is clearly incompatible with the data. The linear fit (solid line), on the contrary, is in agreement with HL predictions. There is no measurable residual static force.

for nylon (see Sect. 6), and they give excellent agreement with sound velocity measurements.

The results for oxidized brass, displayed in Figure 5, are in contradiction with the predictions of reference [16]. There is no significant difference with the behavior of clean brass beads, and an oxidized surface layer does not seem to be responsible for discrepancies with HL. We will comment the behavior of the brass beads at high static forces in Section 6.

The glass and nylon beads follow closely the predictions of HL, although they have the less spherical shapes (see Tab. 1), which seems to contradict the model of reference [15]. For the glass beads, we apply static force up to 600 N. At this force breaking of the beads begins. Before this fracturation, that extends on the scale of the bead diameter, small fractures appear at the contacts. Thus some conical contacts, in the sense of reference [15], probably appear at this stage. Nevertheless, the predictions of

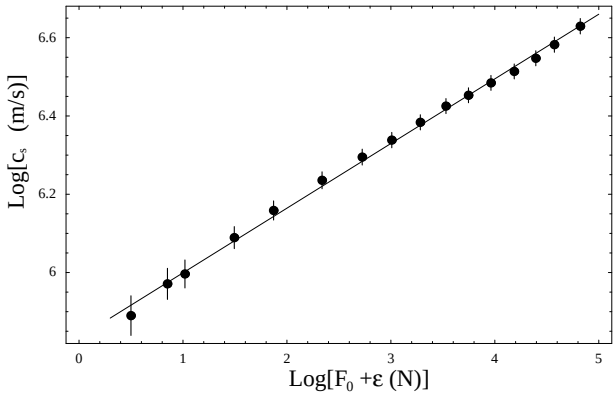

Fig. 5. Same as Figure 2, but for a chain of superficially oxidized brass beads. The static force range is $F_0 \in [2, 124]$ N, and the corresponding sound velocity range $c_s \in [361, 757]$ m/s. The linear fit is in agreement with HL predictions

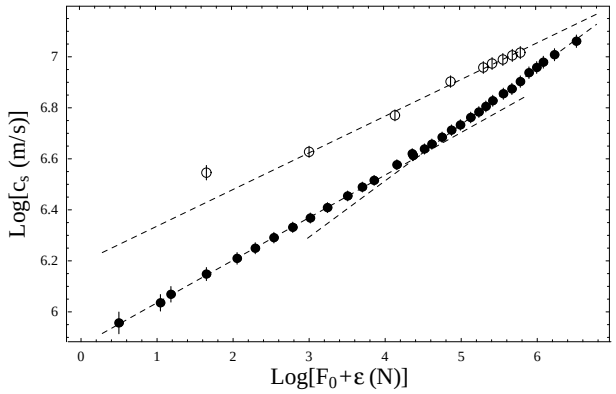

Fig. 6. Logarithmic plot of the sound velocity c_s (in m/s) *versus* the static force applied to the chain $F = F_0 + \varepsilon$ (in N) for a chain of non oxidized brass beads. The static force range is $F_0 \in [3, 690]$ N, and the corresponding sound velocity range $c_s \in [386, 1166]$ m/s. The filled disks show the evolution of the velocity when the static force is *increased*. The data clearly display two linear regimes, corresponding to the HL at low static forces, but with a slope $\alpha_l = 0.22 = 1/4.5$ at higher static forces. The value of the force at the transition, $F_0 \approx 80$ N, corresponds to the onset of plastic yield (see Tab. 5). The empty disks show the evolution of the velocity when the static force is *decreased* from its maximum value. It seems to be linear, too, this time with a slope 1/7. Hysteretic behavior is clearly observed.

HL are still valid despite this strongly inelastic behavior. However, using spherical grains is not fully satisfactory to test this model, which may be relevant for grains of more prismatic shapes, like sand grains.

Figures 5 and 6 show that brass, either oxidized or not, follows closely the Hertz prediction for static forces up to 80 N. We will insist on the characteristic features of brass beads in Section 6, where we show that their behavior at small static force is in contradiction with the model in which De Gennes assumes plastic deformation of microcontacts [17].

The brass beads exhibit a very interesting effect at large static force. Indeed, for forces up to 1200 N in our experiments, the data show an exponent α_l equal to 0.22.

Table 4. Summary of solitary wave velocity measurements, displayed in Figures 7–10. The theoretical value for the power law exponent α_{nl} is 1/6 for the HL and 1/4 for the MHL. See Section 2 for other definitions and Section 5.2 for comments on those results.

	B_H^{th}	B_H^{exp}	α_{nl}^{-1}
Units	m/sN$^{1/6}$	m/sN$^{1/6}$	–
Stainless steel	346.2	350 ± 10	5.9 ± 0.1
Glass	388.4	400 ± 12	6.0 ± 0.1
Brass	256.5	200 ± 20	4.5 ± 0.1
Oxydated brass	256.5	200 ± 20	4.5 ± 0.1
Nylon	230.0	228 ± 7	5.9 ± 0.1

We have conducted experiments on steel beads up to the same value of static force, and Figure 2 shows that for steel beads the HL is still valid. Moreover, when the force is decreased, an hysteretic effect is observed in the brass beads chain. We turn back on the details of this behavior in Section 6, but it is interesting at this stage to compare with the measurements of Duffy and Mindlin [9]. They used steel beads, 3 mm in diameter, arranged in a regular FCC packing. The tolerance is extremely high, $\pm 0.25\,\mu$m and $\pm 1.25\,\mu$m, to be compared with the specifications of our steel beads given in Table 1. Their experiment is clearly in a 3D geometry, even if the length to width ratio is fairly large, around 8. Indeed, they do observe inactive contacts, that is adjacent grains without stress transmission between them, and inhomogeneities in normal forces. The average normal force between adjacent contacts is appreciately greater than in our experiments, because it ranges in $[267, 3563]$ N. They observe a power law with exponent 1/4 at small static force, which means in their experiments $F_0 \leq 1250$ N, and the 1/6 exponent is recovered at higher static force. This is clearly a 3D effect, coming from the progressive activation of the contacts rather than from a modification in their individual behavior. They do not report on any hysteretic effect. This is in complete contrast with our observations for a 1D experiment in which obviously all contacts are active ones.

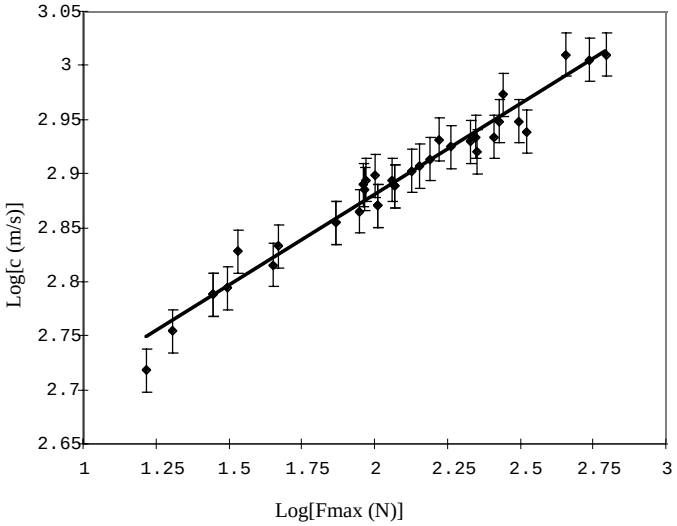

Fig. 7. Logarithmic plot of the solitary wave velocity V (in m/s) *versus* its amplitude F_m (in N) for a chain of stainless-steel beads without any applied static force. The solid line is a linear fit of the data. The values of the exponent α_{nl} and of the proportionality coefficient B_H are to be found in Table 4. The amplitude range is $F_m \in [16, 737]$ N, and the corresponding velocity range $V \in [523, 1025]$ m/s. The data display an excellent agreement with HL predictions

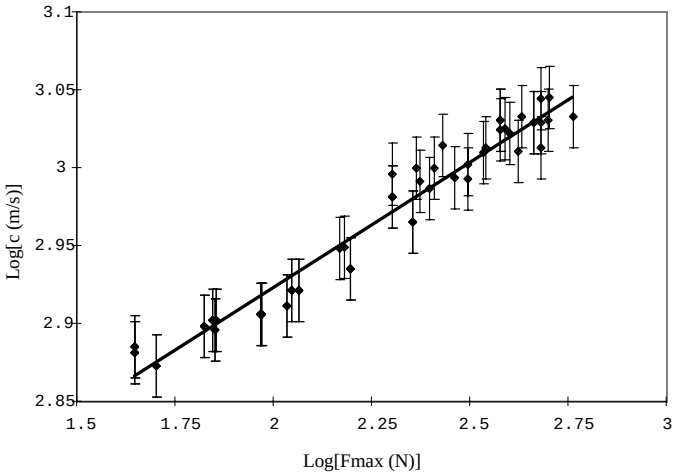

Fig. 8. Same as Figure 7, for a chain of glass beads. The amplitude range is $F_m \in [44, 578]$ N, and the corresponding velocity range $V \in [746, 1110]$ m/s. The data display an excellent agreement with HL predictions

5.2 Velocity of nonlinear solitary waves

In this section, we report on solitary wave velocity measurements in 1D chains of identical beads in the same materials as in the linear case, without any static force applied on the chain. The experimental setup is described in Section 3.3, and in reference [13]. We compare the results to the predictions of HL (18) and MHL (20).

The data are displayed in Figures 7–10, where we plot the solitary wave velocity V as a function of its maximum amplitude F_m in logarithmic scales. The experimental slopes of the linear fits, together with the coefficient of proportionality in (18), are summarized in Table 4. In all cases except brass, the exponent $\alpha_{nl} \approx 1/6$, and the proportionality constant B_H^{exp} clearly follows the HL predictions B_H^{th}.

The results for steel beads, shown in Figure 7, confirm and extend our previous study [13]. The amplitude range is $F_m \in [16, 736]$ N, to be compared to the $[16, 650]$ N range of reference [13]. For glass beads, the amplitude range is almost the same, $F_m \in [44, 578]$ N, and the comparison with HL very favorable, as shown in Figure 8. This is important, because the physical properties that may be relevant for the various versions of MHL are very different in the two types of beads: steel beads are high tolerance ones, made of elastic-plastic material, when glass beads

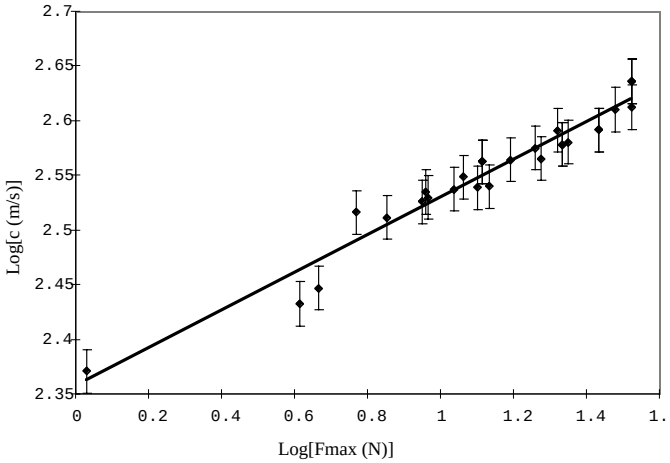

Fig. 9. Same as Figure 7, for a chain of nylon beads. Due to the very low value of the restitution coefficient during the impact with the moving bead (see Sect. 3.3 for details about the nonlinear wave emitter), the amplitude range is very small. It is $F_m \in [1.0, 33]$ N, and the corresponding velocity range $V \in [235, 433]$ m/s. In this range, the data display good agreement with HL predictions

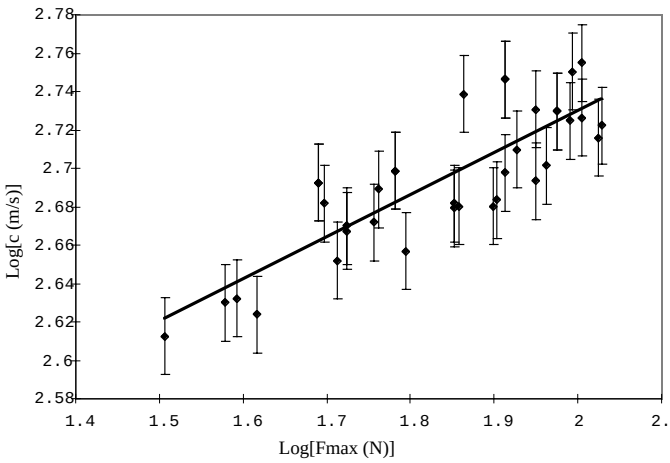

Fig. 10. Same as Figure 7, for a chain of brass beads. The amplitude range is $F_m \in [32, 107]$ N, and the corresponding velocity range $V \in [410, 569]$ m/s. The data are in complete discrepancy either with HL or MHL, because they do not exhibit any power law.

are of poor surface quality, made of brittle material. At the highest amplitudes, the first glass beads in the chain exhibit localized fractures caused by the violence of initial impact. It seems thus that the solitary wave properties are very robust, and persist even when some contacts behave quite far from linear elasticity. We insist on the relevance of this result as a test of Goddard's model, because most of the solitary waves are observed after localized fracturation of the first beads in the chain, which thus exhibits conical asperities rather than flat surfaces at contacts.

The corresponding curve for nylon beads is displayed in Figure 9. There is also good agreement with the HL predictions, but in this case the accessible dynamic range is very small: $F_m \in [1, 33]$ N. Indeed, the restitution coefficient for the impact with the moving bead is very small (see details on nonlinear wave generation in Sect. 3.3) and the amount of transfered energy rather small. We will come back to the behavior of the nylon beads chain in Section 6.

For brass beads there is a very clear discrepancy with the HL. Indeed, as shown by Figure 10, there is actually no power law between the velocity and the amplitude. Velocity measurements indicate that brass beads do not follow at all the HL for nonlinear wave propagation. This point is discussed in Section 6.

5.3 Shape of nonlinear solitary waves

As a last test of the different theoretical models, we compare the shape of experimental solitary waves with the theoretical predictions (21, 22), for the same type of beads. As we said before at the end of Section 4, the description of the complete shape requires the knowledge of the wave velocity for a given amplitude. Nesterenko's theory, based on HL, gives an explicit relation (18) and the shape is completely known once the maximum amplitude is given, without free parameters. Since the three versions of MHL give just the exponent of a power law, not the prefactor, the velocity is not known as a function of the amplitude. For steel, glass and nylon beads, we use the experimental values of the velocity as an input. For brass, there is too much scattering in the data, and we rather use the value predicted by the Hertz theory. With this method, the shape measurements provide a new, independent test of HL and MHL in the nonlinear regime.

In all cases, as shown most clearly by Figure 11, there is an excellent agreement between the experimental points and the profile predicted by the HL, shown as a solid line, and a very clear discrepancy with the MHL, shown by the dashed line. This was already known for steel beads [13], and its no surprise for glass or nylon beads for which the velocity measurements were in good agreement with HL. The behavior of brass beads seems rather strange, in view of the nonlinear waves velocity results shown in Figure 10. In the next section, we try to interpret this seemingly contradictory result.

6 Discussion

In this section, we try to explain the rather complicated behavior of brass beads. We think that plastic deformation of the contacts is responsible for it. Since the literature [29] predicts that nylon beads should be as plastic as brass beads, we also discuss the linear and nonlinear wave propagation, together with an experiment of static compression in nylon beads chain.

Let us first comment the brass beads behavior. As shown by Figure 6, when the applied static force is *increased*, we observe two different regimes for acoustic wave propagation. At small static force, roughly less than 70−80 N, the sound wave velocity follow the HL. At higher

static forces, the power law exponent of sound velocity is rather 0.22 than 1/6, as shown in Figure 6. If we now *decrease* the static force applied on the *same* configuration of the setup, the velocity decreases too, but with a different exponent, very near 1/7. Finally, if we take the beads off the setup, mix them and build a different chain configuration, the HL behavior is recovered at small *increasing* static force. Thus after high deformation of the beads, their behavior is hysteretic. This hysteresis is a strong evidence that plastic deformation of the beads is involved.

The contact between beads (more generally, solids with smooth surfaces) is discussed by Johnson [30]. When the force applied on the beads is small, the behavior of the material is elastic and the deformation is described by Hertz's law. The elastic deformation extends in a very narrow region near the contact point. At higher forces, the deformed region keeps to be narrow, but a small part of it endures irreversible plastic deformation, while the other part still behaves elastically. The plastically deformed region increases with the force. Finally, at very large forces, the plastic deformation extends on a size scale comparable to the beads radius. Let b be the radius of the circular contact area between two adjacent identical beads of radius a. The Hertz's law predicts that

$$b = \left(\frac{3F_0 a}{4\theta}\right)^{1/3}. \tag{24}$$

The mean pressure is thus $\overline{p} = F_0/(\pi b^2)$, and the maximum pressure, at the center of the contact region, is shown to be $p_m = 3\overline{p}/2$. It thus reads

$$p_m = \left(\frac{6F_0\theta^2}{\pi^3 a^2}\right)^{1/3}. \tag{25}$$

An empirical statement fixes the onset of yielding when the maximum pressures reaches $1.6 \times Y$, where Y is the Yield stress of the relevant material. This is called von Mises criterium by Johnson ([30], Sect. 11.5); the limiting force is thus

$$F_0 < F_l \equiv \frac{\pi^3 1.6^3}{6} Y^3 \frac{a^2}{\theta^2}\,. \tag{26}$$

Taking for a the order of magnitude of 1 μm, as for a microcontact, lead to a very small value of F_l. It is clear that plastic behavior of microcontacts is *not* seen in our experiments. The numerical values of F_l, for the different plastic materials used in our experiments, and for identical beads of radius 4 mm, are given in Table 5. For steel, $F_l \approx 1300$ N, which is greater than either the static force applied to the chain (see Sect. 5.1), or the nonlinear waves amplitude (see Sect. 5.2), so that we stay during all experiments in the elastic regime. For brass beads, the numerical value of F_l coincides with the transition from the 1/6 to the 0.22 exponent, shown by Figure 6. Moreover, once the limiting force is exceeded, the chain behavior is hysteretic. It is thus reasonable to think that plastic deformation is responsible for this change in the behavior of brass beads.

Table 5. Limit force for onset of plastic behavior in the contact of two beads of radius 4 mm [see Eq. (26)]. Data for steel and brass are taken from reference [31], data for Nylon are taken from technical documentation of the bead manufacturer.

Signification	Yield stress	Limit force
Symbol	Y	F_l
Unit	N/m^2	N
Stainless steel	6.12×10^9	1260
Brass	1.44×10^9	70
Nylon	10^8	19

In the nonlinear experiments, the impact between the moving tungsten-carbide bead and the chain of brass beads is certainly highly plastic (see Sect. 3.3 and [13] for details on the experimental setup). This causes a large damping of the energy transfered in the chain by the initial impact, during the first stage of wave propagation. In that case, the wave amplitude at the end of the chain is much smaller than its initial amplitude, and its actual travel time differs from what it should have been if its amplitude stay constant and equal to its final value. On the contrary, as shown by Figure 11, the final shape of nonlinear waves that have traveled along a brass bead chain is accurately described by (21), which is the prediction of the HL. We emphasize that the wave is *supposed* to have the velocity given by HL. Of course, their amplitudes are respectively 30 N and 90 N, which is below the onset of plastic yielding. But it is clear from Figure 10 that the measured velocity of waves with a final amplitude in this range, $1.5 \leq \log_{10} F_m \leq 1.95$, do not follow the HL predictions. There is nevertheless no paradox between this result and our previous interpretation of the discrepancies between the nonlinear waves velocity measurements and the HL. The picture of nonlinear wave propagation in brass is as follow: in a first stage, the plastic deformation of contacts is very important, and the wave looses a great amount of energy during its propagation. Then, the contact dynamics is essentially elastic, following HL. The waves observed at the end of the chain thus have a shape which is accurately predicted by (21). The violent impact with the tungsten carbide bead causes rotation of the first brass beads in the chain[1], and thus the contacts between beads are ensured by different parts of the bead surface in different experiments. Since plastic deformations occur in a small part of the beads, the contacts have different history for each solitary wave that is sent in the chain. This may lead to the large, and poorly reproducible, scatter in solitary wave velocity shown in Figure 10.

In the litterature [29], the Yield stress for nylon may vary in a rather large interval. All our experiments show

[1] This rotation of the beads is observed in all experiments, whatever the bead material, except perhaps the nylon beads for which the restitution coefficient is very small. The effect is seen on brass beads only because they exhibit permanent plastic deformation of the contacts.

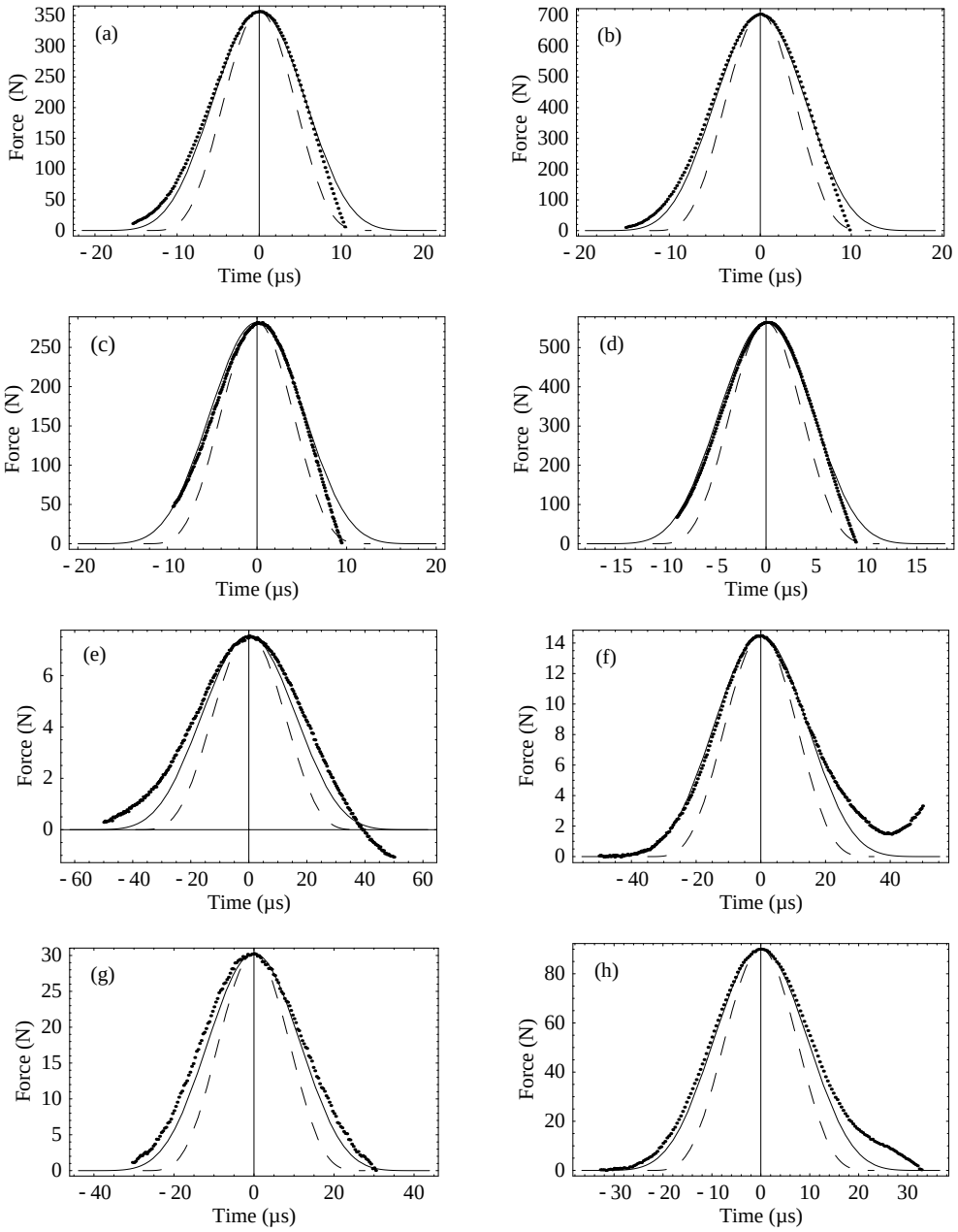

Fig. 11. Shape of solitary wave, where the amplitude in N is shown as a function of time in μs. The graphs respectively correspond to a chain of steel beads (a), (b), glass beads (c), (d), nylon beads (e), (f) and brass beads (g), (h). The dots are experimental points, taken from the digital scope, the solid line displays the HL prediction (21) and the dotted line the MHL prediction (22). For all materials, the agreement is much better with the shape predicted by HL.

that the nylon beads closely follow the HL. The maximum amplitude of nonlinear waves is 33 N, which is slightly greater than the value of F_l, 19 N; nevertheless, nonlinear wave propagation in nylon is described by HL. To study the propagation of acoustic waves, we exert on the chain a static force up to 90 N. The maximum static force is greater than the upper limit for F_l, but we do not see any change in the slope of the linear fit in Figure 4, neither any hysteresis. It seems that the Nylon beads behave elastically in all our experiments. We have verified this fact with a simple experiment, in which we measure the deformation of the chain as a function of the static compression. The displacement of the static force sensor is monitored by an endless screw of thread 1 mm. The nylon beads are so soft that this device, together with the force sensor, may be considered as perfectly rigid. Moreover, the displacement of the sensor is of several millimeters and may be precisely measured. In Figure 12, we display the static force F_0 as a function of $\delta_0^{3/2}$. The linear fit is excellent, providing a direct confirmation of (1). The experimental value of the slope is $1.23 \times 10^8\,\mathrm{N/m^{3/2}}$,

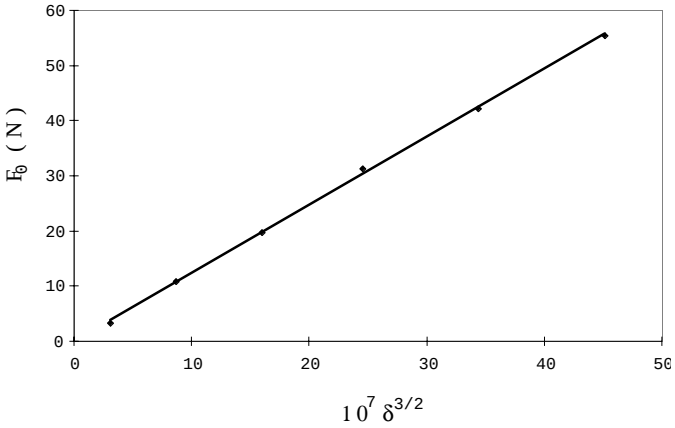

Fig. 12. Plot of the static force F_0, in N, exerted on a chain of nylon beads as a function of the displacement between the centers of adjacent beads, δ_0 in m, to the power 3/2. There are few experimental points, but the linearity is good and the experimental value of the slope is very near the HL predictions.

to be compared to the theoretical value for the HL, which is from the data of Table 2, $(2\theta/3)\sqrt{a/2} = 1.26 \times 10^8$ N/m$^{3/2}$. In the experiment, we do not observe any permanent plastic deformation, although we apply a maximum force of 60 N, greater than F_l for nylon beads. No hysteresis is observed, neither in sound velocity measurements nor in the static experiment. The onset of plastic yielding for the nylon beads seems to extend outside the available static force range in our experiments, which may be caused by the mechanical treatment undergone during their making.

7 Summary and conclusion

Let us summarize our results.

Linear velocity measurements show that the HL describes satisfactorily the behavior of all types of beads, at small static forces. The fact that the behavior of brass beads is not affected by oxidation is in contradiction with the first De Gennes model, that attributes to metallic oxide layers a correction to HL [16]. The Goddard model [15] assumes conical contacts between grains. Although the beads used in our experiments have tolerances that range on one order of magnitude, no significant evolution with the distance to perfect spherical shape is observed. Those observations do not rule out the relevance of this model to assemblies of prismatic grains. But glass beads display a behavior that is fully consistent with HL, on a static force range that extends toward breaking of the beads. Localized fracturation at the contacts happens well before, and inevitably causes contacts between conical asperities, which does not seem to imply any discrepancy with HL. Finally, the fact that for small static forces the behavior of all beads is described by HL is in disagreement with the second De Gennes model [17], which attributes to plastic deformations of microcontacts the difference with pure Hertzian contact. As a simple estimate readily shows, deviations from Hertzian behavior should happen at our first measurements.

Nonlinear measurements confirm those observations, except in the case of brass beads. No discrepancy with HL is observed, even for rather high amplitude waves. Nonlinear waves should nevertheless be more sensitive to the different mechanisms suggested by the different versions of the MHL. Indeed, wave propagation in a chain of beads in contact, but without any constraining force is a purely nonlinear effect, strongly dependent from the contact law between adjacent grains. Moreover, no adjustable parameter is used in the analysis, assuming only HL. Observation of nonlinear solitary waves constitutes thus a very severe test for the HL.

A natural static force scale seems to be the onset of plastic yielding, as shown by the data for brass beads. Below this limit, they behave in close agreement with linear elasticity. At higher static force, the sound velocity evolves with the force as a power law of exponent 0.22 rather than 1/6. Accordingly, the propagation of nonlinear waves in brass beads is strongly affected by plastic deformations at the contacts.

Our observations rule out the microscopic models leading to a modified law of interaction at grain-grain contact, although the Goddard's model should be relevant for prismatic grains. At moderate forces, or for waves of moderate amplitude, plastic materials such as brass display considerable discrepancies with the Hertz law: the exponent in the power laws is not 1/6, an hysteretic behavior is observed in sound velocity measurements when the static force is decreased, and the velocity of nonlinear waves as a function of their amplitudes is not even described by a power law. It seems that one should not consider plastic deformation of a microscopic scale (in the sense of De Genne's microcontacts), but rather on a length scale comparable to the one that arise in the Hertz theory of contact.

We gratefully acknowledge technical help from D. Bouraya during the making of the setup.

References

1. K. Iida, Bull. Earthquake Res. Inst. (Tokyo) **16**, 131 (1938).
2. K. Iida, Bull. Earthquake Res. Inst. (Tokyo) **17**, 783 (1939).
3. P. Talwani, A. Nur, R.L. Kovach, J. Geophys. Res. **78**, 6899 (1973).
4. C.W. Thurston, H. Deresiewicz, J. Appl. Mech. ASME **26**, 251 (1959).
5. N. Warren, O.L. Anderson, J. Geophys. Res. **78**, 6911 (1973).
6. Chu heng Liu, S.R. Nagel, Phys. Rev. Lett. **68**, 2301 (1992).
7. Chu heng Liu, S.R. Nagel, Phys. Rev. B **48**, 15646 (1993).
8. L.D. Landau, E.M. Lifshitz, *Theory of elasticity* (Pergamon Press, Oxford, 1986).
9. J. Duffy, R.D. Mindlin, J. Appl. Mech. **24**, 585 (1957).

10. V.F. Nesterenko, J. Appl. Mech. Tech. Phys. **24**, 567 (1983).
11. V.F. Nesterenko, J. Phys. IV Colloq. France 729 (1994).
12. A.N. Lazaridi, V.F. Nesterenko, J. Appl. Mech. Tech. Phys. **26**, 405 (1985).
13. C. Coste, E. Falcon, S. Fauve, Phys. Rev. E **56**, 6104 (1997).
14. C. Coste, E. Falcon, S. Fauve, in *Des géomatériaux aux ouvrages*, edited by C. Petit, G. Pijaudier-Cabot, J.-M. Reynouard (Hermès, Paris, 1995), p. 33.
15. J.D. Goddard, Proc. R. Soc. Lond. A **430**, 105 (1990).
16. P.G. de Gennes, Europhys. Lett. **35**, 145 (1996).
17. P.G. De Gennes, Lectures of the "Collège de France" held at "École Centrale de Lyon", 1997.
18. H.J. Hermann, D. Stauffer, S. Roux, Europhys. Lett. **3**, 265 (1987).
19. S. Roux, D. Stauffer, H.J. Hermann, J. Phys. France **48**, 341 (1987).
20. D. Stauffer, H.J. Hermann, S. Roux, J. Phys. France **48**, 347 (1987).
21. A. Drescher, G. de Josselin de Jong, J. Mech. Phys. Solids **20**, 337 (1972).
22. T. Travers, M. Ammi, D. Bideau, A. Gervois, J.C. Messager, J.P. Troadec, J. Phys. France **49**, 939 (1988).
23. J.N. Roux, in *Proceedings of the Saint-Venant Symposium*, edited by J. Salençon (Presses de l'Ecole Nationale des Ponts et Chaussées, Paris, 1997), p. 577.
24. J.N. Roux, in *Powders and Grains 97*, edited by R.P. Behringer, J.T. Jenkins (A.A. Balkema, Rotterdam, 1997).
25. G.E. Martin, J. Acoust. Soc. Am. **36**, 1496 (1964).
26. L.G. Merkulov, A.V. Kharitonov, Sov. Phys. Acoust. **5**, 183 (1959).
27. K. Walton, Geophys. J. R. Astr. Soc. **43**, 293 (1975).
28. G. Rowlands, E. Infeld, *Nonlinear waves, solitons and chaos* (Cambridge university Press, Cambridge, 1990).
29. D.R.H. Jones, M.F. Ashby, *Matériaux* (Dunod, Paris, 1991).
30. K.L. Johnson, *Contact mechanics* (Cambridge university Press, Cambridge, 1992).
31. D.E. Gray, *American Institute of Physics handbook*, 3rd ed. (Mac Graw Hill, New York, 1972).
32. R.C. Weast, *CRC handbook of chemistry and physics*, 60th ed. (CRC Press, New York, 1979).